

Circuit model of uni-traveling carrier photodiode with high power and enhanced bandwidth technique

Senjuti Khanra · Abhirup Das Barman

Received: 24 September 2014 / Accepted: 3 December 2014 / Published online: 13 December 2014
© Springer Science+Business Media New York 2014

Abstract An electrical equivalent circuit model of InGaAs/InP uni-travelling carrier photodiode (UTC-PD) is presented. The model is suitable to be built on any electrical circuit simulator to optimize the design parameters of the device. Its performance in terms of bandwidth, linearity, third order inter-modulation distortion and output photo current are investigated. Simulation techniques to measure inter-modulation distortion products and linearity are given in detail. The result obtained by the modeling technique is validated through a comparison with the reported experimental results. It is shown that 3 dB cutoff frequency and output photocurrent can be substantially improved by inserting a small inductance in series with the load together with choosing an optimum absorption layer width in UTC-PD. This technique does not sacrifice the device linearity to a large extent.

Keywords Circuit model · Frequency response · Photodiode · Inter-modulation

1 Introduction

The 60, 90 and 120 GHz millimeter wave (MMW) bands are of great interest for wireless data transmission as these frequency bands are ‘license free’ (Shi et al. 2001). MMW signal can be easily transported by radio over fiber (ROF) (Yao 2012) from central to the multiple remote antenna unit (RAU) base stations (Hekkala et al. 2010). UTC photodiode-based photonic-wireless transmitter has the potential to be a key component for 75–180 GHz wireless transmission (Shi et al. 2001). The MMW transmitter (Shi et al. 2001) consists of a

S. Khanra · A. D. Barman (✉)
Institute of Radio Physics and Electronics, University of Calcutta, 92, Acharya Prafulla Chandra Road,
Kolkata 700009, W.B., India
e-mail: abhirup_rp@yahoo.com

S. Khanra
e-mail: senjuti.physics@gmail.com

S. Khanra · A. D. Barman
ITRA project “Mobile Broadband Service Support over Cognitive Radio Networks”, IRPE-CU,
Kolkata, India

high-power and large band width photodiodes, built-in amplifier and antenna on the same guiding structure radiates signal directly to the end user. Such approach facilitates microcellular system (Zhu 2011); with several hundred meters diameter communication range provides higher spectrum utilization and capacity. In order to integrate UTC-PD with other photonic and radio frequency (RF) components and to optimize the system performance an electrical circuit model of the device is required. Additionally, the device must have good linearity. In order to gain insight to all the above factors it is important to have a tool to analyze the device performance in particular, to predict harmonics and inter-modulation distortion products (IMD_3). Hence techniques for high bandwidth UTC-PD must be investigated without sacrificing its high power.

Efforts have largely been devoted to optimize the device performance through various experiments (Pan et al. 2010; Ishibashi et al. 2000; Ito et al. 2004; Chtioui et al. 2012). However, till date very few comprehensive physics based circuit models of UTC-PD have been reported. Brief accounts of the shortcoming of the existing models (Beling et al. 2008; Kuo et al. 2009) are as follows: Beling et al. (2008) proposed an equivalent circuit of UTC-PD to analyze frequency characteristics of third order inter-modulation distortion product at high photocurrents. Transit-time effects of carriers have not been considered in their work. As a result dependency of bandwidth on absorption layer width could not be shown. Kuo et al. (2009) in their work presented an equivalent circuit model of UTC-PD to study the internal dynamic behaviors particularly bandwidth enhancement effect of GaAs-AlGaAs based UTC-PD under zero bias by combining transit time and RC delay time where R is the load resistance and C is the capacitance at the junction. No results have been found on inter modulation distortion and linearity study. To achieve high photocurrent thick absorption layer (1,200 nm) may be employed but this limits the linearity and bandwidth to less than 30 GHz (Chtioui et al. 2012). A solution is urgently required to achieve high photocurrent as well as high bandwidth of the device. On the other hand researchers have found that independently large bandwidth and high photocurrent can be achieved using waveguide photodiode (WGPD) structure. This is reported in Lasaosa et al. (2004). However photocurrent can still be limited by saturation effect of the carriers. Maintaining a constant optical power along the device in an integrated amplifier based WGPD (Piprek et al. 2003) problem can be largely solved but at the cost of high amplified spontaneous emission noise (ASE) during the pre-amplification process. In this method the slow movement of holes does not restrict the carrier speed due to adaptation of very thin absorption layer of the device. In UTC-PD, the problem of slow movement of holes is eliminated by a diffusion block layer near the p-contact.

In this work, a comprehensive UTC-PD equivalent circuit model is developed from the simple integral rate equation (Ishibashi et al. 2001) involving electron and hole movement in the device. Incorporating the effect of self-induced field (E_{ind}) (Ishibashi et al. 2001), the total frequency response of the device is determined. From the total frequency response sub-blocks are formed which are implemented by the circuits containing current controlled, voltage controlled sources and by other passive elements. The circuit implementation of UTC-PD and simulation techniques to measure inter-modulation distortion and frequency response are discussed in detail. Optimum absorption layer width of the device can be obtained from the intersection curves of 3 dB cutoff frequency and output photocurrent. It is shown here that by inserting an inductor in series with load resistance a substantial improvement of 3 dB cutoff frequency can be achieved without sacrificing the output photocurrent and device linearity to a large extent.

The paper is organized as follows: Section 2 is devoted to circuit modeling and simulation methods. Section 3 reports the results on some important characteristics of UTC-PD and the bandwidth enhancement effect due to inductor. Conclusions are drawn in Sect. 4.

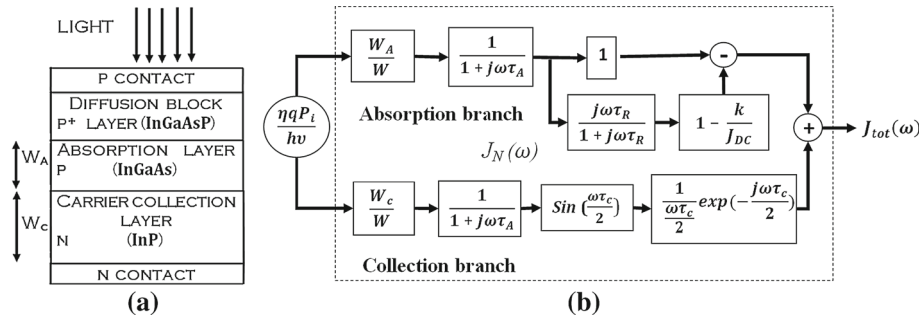


Fig. 1 **a** Schematic of top illuminated UTC-PD and **b** different mathematical subsections of UTC-PD

2 Circuit model and simulation techniques

2.1 Circuit modeling of UTC-PD

Schematic of UTC-PD is shown in Fig. 1a. Details of the device structure can be found in Ishibashi et al. (2001).

The normalized frequency response of the electron injection current from the absorption layer to the collection layer can be calculated as (Ishibashi et al. 2001)

$$\begin{aligned}
 J_N(\omega) &= \frac{J_{tot}(\omega)}{J_{DC}} \\
 &= \frac{W_A}{W} \left[\frac{1}{1 + j\omega\tau_A} \right] \cdot \left[1 - \frac{j\omega\tau_R}{1 + j\omega\tau_R} \left(1 - \frac{k}{J_{DC}} \right) \right] \\
 &\quad + \frac{W_C}{W} \left[\frac{1}{1 + j\omega\tau_A} \right] \text{Sinc} \left(\frac{\omega\tau_C}{2} \right) \exp \left(-\frac{j\omega\tau_C}{2} \right) \quad (1)
 \end{aligned}$$

where the output dc current J_{DC} is $\frac{\eta q P_i}{h\nu}$, the constant term k used to derive Eq.(1) is given by $(q\mu_n n_o E_{ind})/2$ and the efficiency η is (Leavitt and Bradshaw 1991) $(\exp(-\frac{W_A}{L_e}) - \exp(-\alpha W_A))$ considering only drift motion of photo generated minority electrons in the n-type InP collection layer. The descriptions of other device parameters used in Eq. (1) are given in Table 1. In deriving Eq. (1) we have taken into account the self induced electric field (Ishibashi et al. 2001) which develops due to accumulation of holes by the diffusion block layer. This causes the absorption layer quasi-neutral. Due to this field the UTC-PD can be operated even at zero bias condition (Ito et al. 2004) which is not possible in a conventional photodiode. Normalized frequency response of UTC-PD can be represented by small subblocks in Fig. 1b. The upper branch in Fig. 1b represents the absorption layer response due to travelling time of electrons in the absorption layer and dielectric relaxation time of the majority carrier holes and the lower branch contains terms involving travelling time of electrons in the absorption and collection layers. Careful analysis of Eq. (1) shows that it contains some constant and frequency dependent terms written as sum of the product. The basic subsystem elements which construe Eq. (1) are of the following types:

$$J_{out}(\omega) = J_{in} \cdot K, K = \text{constant} \dots \quad (2a)$$

$$J_{out}(\omega) = J_{in} \frac{1}{1 + j\omega\tau} \dots \quad (2b)$$

Table 1 Parameter values used for simulation

Symbols	Parameters	Values
W_A	Absorption layer width	200 nm
W_C	Collection layer width	300 nm
p_o	Absorption layer doping density	10^{24} m^{-3}
n_o	Collection layer doping density	10^{22} m^{-3}
τ_A	Absorption layer travelling time	8.3 ps
τ_C	Collection layer travelling time	46.15 ps
τ_R	Dielectric relaxation time in W_A	0.049 ps
E_{ind}	Max. self-induced electric field	12 kV/cm

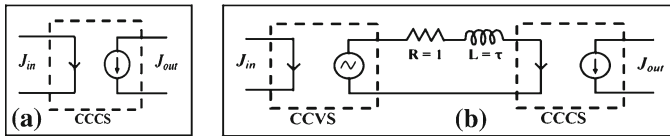


Fig. 2 Circuit realization of different functional block of UTC-PD

$$J_{out}(\omega) = J_{in} \frac{j\omega\tau}{1 + j\omega\tau} \dots \tag{2c}$$

$$J_{out}(\omega) = J_{in} \cdot \exp(-j\omega\tau) \dots \tag{2d}$$

The subsystem blocks given by Eqs. (2a)–(2d) can be realized following the basic rules of circuit theory. The first block in Eq. (2a) can be realized by a current controlled current source (CCCS) with gain K. This is shown in Fig. 2a. The term in Eq. (2b) can be realized by the sub circuit in Fig. 2b. In Fig. 2b we use current controlled voltage source represented by CCVS of unit gain converting input current to an equivalent voltage J_{in} ; CCVS is followed by an R-L circuit to obtain an output current $\frac{J_{in}}{1+j\omega\tau}$, where τ is equal to L Henry. The output of this block is connected to CCCS because next sub-block is driven by the current. The subsystem in Eq. (2c) can also be built in a similar way as in Eq. (2b) except inductor (L) is replaced by capacitor (C) equal to τ Farad. Finally, the term in Eq. (2d) can be implemented by a CCCS with a delay τ s. Multiplicative and additive sub blocks are connected in series and parallel respectively. The negative sign can be realized by connecting the positive end of one sub-circuit with the negative end of the other sub-circuit block. Using the rules for building basic subcircuit blocks shown in Fig. 2 the complete equivalent circuit model of UTC-PD is implemented from Eq. (1). Complete circuit model is shown in Fig. 3a. Here electron-hole pair generation due to uniform optical excitation is represented by a current source. The absorption region is modeled with series inductance L representing the carrier transit time (τ_A) and C representing the relaxation time (τ_R) of photo-generated holes in the absorption layer.

2.2 Linearity and inter-modulation distortion (IMD_3)

Linearity and high optical-power handling are the key requirements for high-performance UTC-PD based photonic wireless transmitter applications. Thus, from the design standpoint, it is important to have tools able to evaluate the performance of UTC-PD and in particular, predict harmonics and IMD_3 generation. The two modulated signals are combined at the

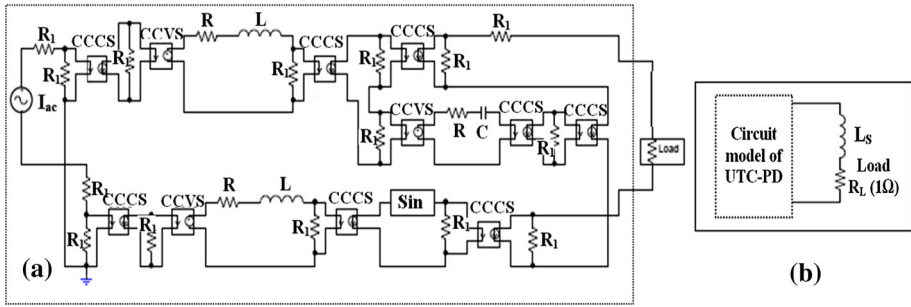


Fig. 3 a Equivalent circuit model of UTC-PD ($R, R_1 = 1\Omega$) and b inductance L_S in series with load

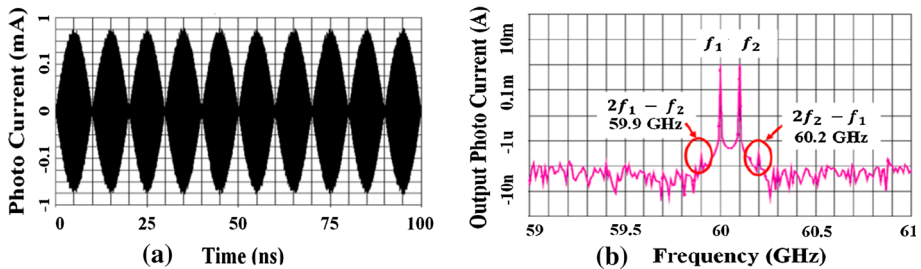


Fig. 4 a Time cycles and b spectrum of inter-modulation product

UTC-PD and the generated inter-modulation products give the measure of linearity. In order to investigate IMD_3 in simulation, two tone input signals I_1 and I_2 with frequency f_1 and f_2 (typically assumed here as 60GHz (f_1) and 60.1GHz (f_2) respectively with 100MHz separation) are fed to the UTC-PD. A transient a.c. analysis is carried out for a signal of duration 0–100ns. For accurate estimation of the frequency, at least ten cycles of 100MHz (difference between two input MMW frequencies) equivalent to 10ns time span must be taken as shown in Fig. 4a. Otherwise, error in frequency estimation will occur. Then Fourier Transform of these time cycles is performed to obtain spectrum of inter-modulation products. This is shown in Fig. 4b. Employing this method accurate simulation of inter-modulation distortion can be found out.

2.3 Bandwidth enhancement technique

Increased thickness of the absorption layer provides high photocurrent but it reduces the bandwidth of the device. To enhance the bandwidth we propose to connect a peaking inductance L_S in series with the load as shown in Fig. 3b. This may be easily implemented in integrated circuit fabrication of the device. This is a well known technique of increasing bandwidth in electronic video circuit. In integrated circuit solution, this additional inductance may be incorporated by means of short-end coplanar waveguide (CPW) stub (Simons 2001), which can also act as impedance transformer (Ito et al. 2003) to the antenna input.

3 Results and discussions

The electrical circuit model of UTC-PD shown in Fig. 3a is implemented in Capture CIS OrCAD_10.5 simulation software. The device parameter values used for circuit simulation are listed in Table 1.

3.1 Output photocurrent and bandwidth enhancement by inductor peaking

To obtain 3 dB cut off frequency from the circuit model of the device, an a.c. sweep from 10 to 1,000 GHz is applied to the input of the circuit shown in Fig. 3a. Input power is kept fixed at 0 dBm. The 3-dB cutoff frequency is noted down for each absorption layer width of the device. The solid black circles and solid black diamond points in Fig. 5 show the 3-dB cutoff frequencies (f_{3dB}) and output photocurrent respectively at different absorption width. The analytical plot of f_{3dB} (Ito et al. 2004) is shown by green squares connecting line in Fig. 5. The output photocurrent is the responsivity times the input power. The analytical output current versus absorption layer width is shown by blue connecting circles in Fig. 5. There is a tradeoff between output photocurrent and 3 dB bandwidth of the device. As f_{3dB} increases with increase in absorption layer width the output photo current decreases. The circuit model of UTC-PD provides a tool to optimize bandwidth and output photocurrent with respect to absorption layer thickness and other device parameters. Experimentally (Ishibashi et al. 2001) obtained f_{3dB} at 220 and 90 nm absorption layer width (W_A) shown by red stars is plotted in Fig. 5 and a close match between experimental and simulation results is found. When peaking inductance $L_S (= 5 \text{ pH})$ is incorporated in series with the load (refer to circuit model in Fig. 3b), the f_{3dB} point increases (shown by open red circles) but photocurrents remain same (values are superimposed on black diamond points) as shown in Fig. 5. The simulation results are given in Table 2. We see from Table 2 that with $L_S = 5 \text{ pH}$, at 300 nm absorption width, the bandwidth enhancement is 186 GHz when photocurrent is nearly 0.5 mA.

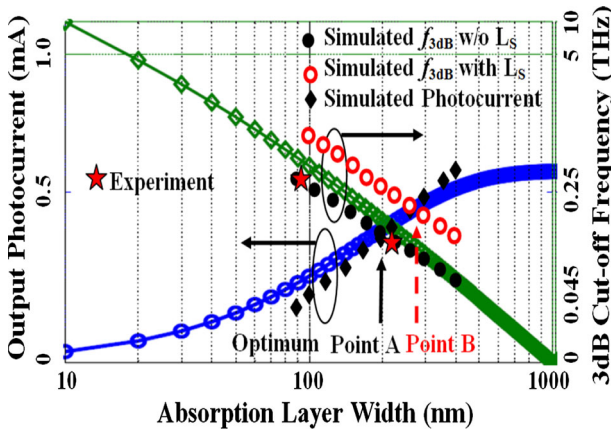


Fig. 5 Photocurrent and cutoff bandwidth at different absorption layer width (W_A) without and with L_S (5 pH). (Color figure online)

Table 2 Simulation results obtained from Fig. 5

Absorption layer width (W_A) in nm	Photocurrent in mA	Inductor value (L_S) in pH			
		0	1	1.5	5
		f_{3dB} in GHz for different L_S			
180	0.312	141	360	375	385
200	0.348	121	302	322	335
300	0.5023	67.5	127	162	186
400	0.6224	43.8	57.5	80	120

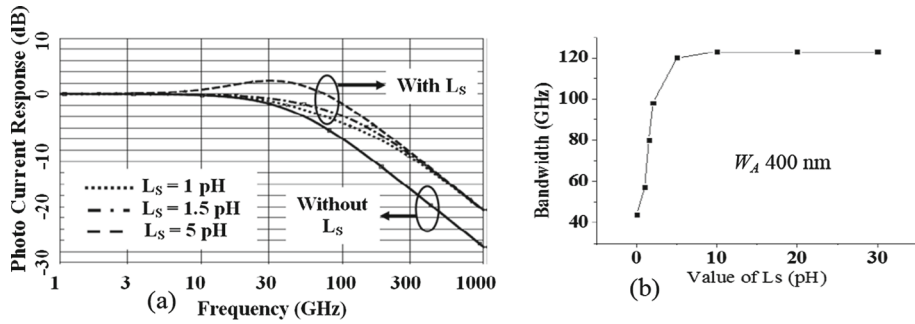


Fig. 6 **a** Frequency response and **b** bandwidth of UTC-PD with different L_S

Frequency response of UTC-PD obtained from the circuit model for different values of L_S is shown in Fig. 6a. Placement of inductor in series with load causes a series resonance in the circuit. This is called inductor peaking. The resonant frequency extends the intrinsic (that without an inductor) 3 dB cutoff frequency of the device as shown in Fig. 6a. However, it is found that the limited range of the inductor between 1 and 5 pH is effective in doing so. Inductor value more than 5 pH causes a higher resonance peak and effectively does not increase the bandwidth further. Bandwidth versus inductor values are plotted in Fig. 6b. It is earlier shown that insertion of L_S does not increase the photocurrent. Since 3 dB bandwidth versus W_A plot in Fig. 5 shifts towards right when L_S is present we obtain a new optimum W_A corresponding to the intersection point 'B' between photocurrent and new 3 dB bandwidth. If absorption layer width W_A is designed at this new optimum point 'B' then larger bandwidth and higher photocurrent can be achieved as shown in Fig. 5.

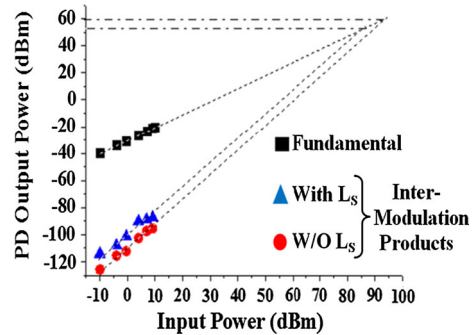
3.2 Inter-modulation distortion (IMD_3) from the circuit model

Simulation technique to measure inter-modulation products is discussed with detail in Sect. 2. As shown in Fig. 4b, for two fundamental frequencies at 60 GHz (f_1) and 60.1 GHz (f_2) the inter-modulation products are found at 59.9 GHz ($= 2f_1 - f_2$) and 60.2 GHz ($= 2f_2 - f_1$) at the output. The amplitude levels of the input current sources at f_1 and f_2 are same and they are varied from 10 to 150 mA. For each input the amplitude of IMD_3 's are noted. Fundamental (P_0) and IMD_3 (P_{03}) powers at the output are plotted in Fig. 7 and imaginary point of intersection between P_0 and P_{03} known as third order intercept point (IP_3) is found out. Then inserting L_S ($= 5$ pH) at the output load, IMD_3 is found out in a similar way for an absorption layer width 400 nm. IP_3 without L_S is 60 dBm and with $L_S = 5$ pH is 56 dBm which is within the acceptable limit.

4 Conclusion

A physics based comprehensive circuit model of InGaAs/InP UTC-PD is developed. The result is validated through a comparison with the reported experimental data. Simulation techniques to measure linearity and inter-modulation products are given in detail. We have shown a method by inserting a small inductance in the range 1–5 pH in series with the load gives higher photocurrent and three fold improvement in the bandwidth provided the absorption layer width is chosen optimally. Moreover, insertion of inductor does not sacrifice

Fig. 7 IP_3 of UTC-PD with and without L_S



the linearity of the device to a large extent. The circuit model developed here can be useful to optimize different UTC-PD parameters and provides a common platform for simulation of UTC-PD with other RF and optoelectronic devices by electronic design automation (EDA) tools.

Acknowledgments The work is undertaken as part of Information Technology Research Academy (ITRA), Media Lab Asia project entitled “Mobile Broadband Service Support over Cognitive Radio Networks”.

References

- Beling, A., Pan, H., Chen, H., Campbell, J.C.: Linearity of modified uni-traveling carrier photodiodes. *J. Lightw. Technol.* **26**(15), 2373–2378 (2008)
- Chtioui, M., Lelarge, F., Enard, A., Pommereau, F., Carpentier, D., Marceaux, A., Dijk, F.V., Achouche, M.: High responsivity and high power UTC and MUTC GaInAs-InP photodiodes. *IEEE Photonics Tech. Lett.* **24**(4), 318–320 (2012)
- Hekkala, A., Lasanen, M., Harjula, I., Vieira, L.C., Gomes, N.J., Nkansah, A., Bittner, S., Diehm, F., Kotzsch, V.: Analysis of and compensation for non-ideal RoF links in DAS. *IEEE Wirel. Commun.* **10**, 1284–1536 (2010)
- Ishibashi, T., Furuta, T., Fushimi, H., Kodama, S., Ito, H., Nagatsuma, T., Shimizu, N., Miyamoto, Y.: InP/InGaAs uni-traveling-carrier photodiodes. *IEICE Trans. Electron.* **E83-C**(6), 938–949 (2000)
- Ishibashi, T., Furuta, T., Fushimi, H., Ito, H.: Photoresponse characteristics of uni-traveling-carrier photodiodes. *Proc. SPIE Phys. Simul. Optoelectron. Dev. IX San Jose* **4283**, 469–479 (2001)
- Ito, H., Nagatsuma, T., Hirata, A., Minotani, T., Sasaki, A., Hirota, Y., Ishibashi, T.: High-power photonic millimeter wave generation at 100 GHz using matching-circuit-integrated uni-travelling-carrier photodiodes. *IEEE Proc. Optoelectron.* **150**(2), 138–142 (2003)
- Ito, H., Kodama, S., Muramoto, Y., Furuta, T., Nagatsuma, T., Ishibashi, T.: High-speed and high-output InP-InGaAs uni-traveling carrier photodiodes. *IEEE J. Sel. Top. Quantum Electron.* **10**(4), 709–727 (2004)
- Kuo, F.-M., Hsu, T.-C., Shi, J.-W.: Strong bandwidth-enhancement effect in high-speed GaAs/AlGaAs based uni-traveling carrier photodiode under small photocurrent and zero-bias operation. In: *Proceedings of LEOS Annual Meeting, TuB3, Belec-Antalya*, pp. 141–142 (2009)
- Lasaosa, D., Shi, J.-W., Pasquariello, D., Gan, K.-G., Tien, M.-C., Chang, H.-H., Chu, S.-W., Sun, C.-K., Chiu, Y.-J., Bowers, J.E.: Traveling-wave photodetectors with high power-bandwidth and gain-bandwidth product performance. *IEEE J. Sel. Top. Quantum Electron.* **10**(4), 728–741 (2004)
- Leavitt, R.P., Bradshaw, J.L.: Transit time effects on photocurrent spectra of multiple quantum well diodes. *Appl. Phys. Lett.* **59**(19), 2433–2435 (1991)
- Pan, H., Li, Z., Campbell, J.C.: High-power high-responsivity modified uni-traveling-carrier photodiode used as V-band optoelectronic mixers. *J. Lightw. Technol.* **28**(8), 1184–1189 (2010)
- Piprek, J., Pasquariello, D., Lasaosa, D., Bowers, J.E.: Novel waveguide photodetectors on InP with integrated light amplification. *Proc. Electrochem. Soc.* **2003**(4), 1–8 (2003)
- Shi, J.-W., Huang, C.-B., Pan, C.-L.: Millimeter-wave photonic wireless links for very high data rate communication. *NPG Asia Mater.* **3**, 41–48 (2001)

Simons, R.N.: Coplanar Waveguide Circuits, Components, and Systems. Wiley, New York (2001)

Yao, J.: A tutorial on microwave photonics, Research Highlights. IEEE Photonics Soc. Newsl. **26**, 5–12 (2012)

Zhu, H.: Performance comparison between distributed antenna and microcellular systems. IEEE J. Sel. Areas Commun. **29**(6), 1151–1163 (2011)